A Tetrakis(terpyridine) Ligand Based Cobalt(II) Complex Nanosheet as a Stable Dual-Ion Battery Cathode Material

Yurong Liu, Wenwen Deng, Zhengong Meng, and Wai-Yeung Wong**

Dr. Y. R. Liu, Prof. W.-Y. Wong
The Hong Kong Polytechnic University Shenzhen Research Institute
Shenzhen 518057, P.R. China.
E-mail: wai-yeung.wong@polyu.edu.hk
Dr. Y. R. Liu, Dr. W. W. Deng, Prof. W.-Y. Wong
Department of Applied Biology and Chemical Technology
The Hong Kong Polytechnic University
Hong Hom, Hong Kong, P.R. China.
Dr. Y. R. Liu, Dr. Z. G. Meng, Prof. W.-Y. Wong
Institute of Molecular Functional Materials and Department of Chemistry
Hong Kong Baptist University
Waterloo Road, Kowloon Tong, Hong Kong, P.R. China.

E-mail: mengzg@szu.edu.cn
Prof. W.-Y. Wong
Hong Kong Baptist University Institute of Research and Continuity Education, Shenzhen
Virtual University Park, Shenzhen 518057, P.R. China.

Keywords: metal-organic nanosheets, layered structures, cathode materials, dual-ion batteries, terpyridine

Inspired by the flexibility of the bottom-up approach in terms of selecting molecular components and thus tailoring functionalities, a brand-new terpyridine derivative (1,2,4,5-tetrakis(4-(2,2':6',2"-terpyridyl)phenyl)benzene) (**Tetra-tpy**) is synthesized and coordinated with Co(II) ion to self-assemble into a novel nanosheet **Co-Sheet** by a facile interface-assisted synthesis. The bis(terpyridine)-Co(II) complex nanosheet formed not only shows good stability, but also features the layered structure and rich electrochemical activity inherited from the embedded Co(terpyridine)$_2$ motif. Thus, **Co-Sheet** can serve as a cathode material for a dual-ion battery prototype, which exhibits a high utilization of redox-active sites, good cycling stability and rate capability, thus expanding the potential application of this kind of easily prepared metal-complex nanosheets in the field of energy storage.

1. Introduction

Since the successful isolation of graphene,[1] two-dimensional (2D) polymers, such as nanosheets have attracted increasing attention thanks to their unique physical, electronic and chemical properties originated from their nature of electron confinement in two dimensions. To expand this nascent field in terms of ultrathin architectures and then meet the demands in various application fields, a series of graphene-like 2D materials, including Mxenes,[2,3] metal oxides,[4,5] and metal hydroxides[6,7] were investigated. The declaration of band gap transition in single-layer molybdenum disulfide[8] further boosted the development of the transition metal dichalcogenides (TMD).[9,10] Most of the aforementioned 2D nanosheets are created via top-down approach, which mainly involves chemical[11–13] or mechanical[14] isolation from bulky mother crystals. Although the top-down method can be used to synthesize high-quality monolayers with clean surface, it suffers from getting small size domain in the nanosheets and complicated post-treatment.

Another building block-based bottom-up approach, which is to rationally synthesize nanoscopic crystallites directly from atomic, ionic, and molecular modules, can be more flexible to design the 2D material structures. Moreover, the prepared sheets can be deposited on various substrates layer-by-layer.[15–18] The representative bottom-up nanosheets mainly include 2D metal-organic frameworks (MOFs)[19,20] and 2D covalent-organic frameworks (COFs).[21,22]

As the complexation between 2,2':6',2''-terpyridine (tpy) and metal ion can be spontaneously and rationally accomplished and there is a good balance between reversibility and robustness, tpy and metal ion are likely to be building blocks of the coordination nanosheets with suitable robustness.[23] A pioneer work on the single- or few-layer of tpy-metal complex nanosheets with focus on the gas-liquid interface-mediated synthesis, structural analysis and transmetalation process was conducted by Schlüter and co-workers.[24–

[26] Nishihara and co-workers studied the electrochromism[27] and photo-functionality of tpy-metal complex nanosheets.[28] As a further study on this type of tpy-metal complex nanosheets, the article presented here examines their electrochemical functionality. Considering that: 1) the electrochemically active tpy-metal motifs were embedded in this kind of nanosheets, and 2) the rigidity of the network structure usually offers excellent stability, which is essential to the long-term use of an energy storage system, and 3) the layered structure could promote the transport of both the ions and electrons in the stacking orientations and inside the layers,[29] the tpy-metal complex nanosheets may be applied as a battery electrode. Most of the widely studied cathode materials are inorganic compounds including XMene and graphitic cathode materials.[30] However, the capacity limit hinders their further development. Besides, the inserted anions could increase the cell volume of the cathode materials, and may lead to structural alteration and degradation, thus resulting in poor reversibility.[31] On the other hand, organic cathodes could exhibit high safety, low carbon footprint, and ease of recycle.[32–34] Speer *et al*. reported an organic polymer as the cathode, exhibiting a high capacity of 66 mA h g^{-1}. However, its capacity was down to around 20 mA h g^{-1} after 100 cycles at 1 C, reflecting the poor stability.[35] MOFs such as Fe_2(dobpdc) (dobpdc^{4-} = 4,4′-dioxidobiphenyl-3,3′-dicarboxylate) as cathode material have been reported to show a good reversibility for at least 50 cycles,[36] while certain organic cathodes still suffer from swelling upon insertion or phase instability.[37–39]

In view of this background, cathode material with a high reversibility is yet to be explored. 2D materials, which can electrochemically accommodate anions due to their distinctive layered structure, are a promising candidate. Recently, a few-layer graphene was reported to show a high specific capacity and excellent cycling stability. Nevertheless, a high processing temperature is necessary.[40] Herein, we report a stable and easily-prepared bis(tpy) cobalt(II) complex nanosheet based on the novel 1,2,4,5-tetrakis(4-(2,2':6',2"-terpyridyl)phenyl)-benzene (**Tetra-tpy**) ligand and use it as a dual-ion cathode material. The

bottom-up 2D metal complex nanosheet display structural diversity and tunability. Yet, the study on using it as the dual-ion cathode is scarce. Of particular emphasis in this article is to open up a new prospect towards the applicability of this kind of layered metal complex nanosheets as useful nanomaterials in battery system as well as to pave the way to developing stable dual-ion cathode materials.

2. Results and Discussion

2.1. Synthesis and properties of Co-sheet

The ligand **Tetra-tpy** features four functional terpyridines and its spontaneous coordination with Co^{2+} ions could result in a nanosheet **Co-sheet** with the topological structure shown in **Figure 1** (the counter anions are omitted for clarity). A liquid-liquid interface was created with a dichloromethane (CH_2Cl_2) solution of **Tetra-tpy** as the lower layer and an aqueous solution of excessive cobalt dichloride as the upper layer to lead to the coordination reaction.[41] The resultant yellow **Co-sheet** with metallic luster was visible and completely covered the whole interface (**Figure 2**a). To make a contrast, the one-phase synthesis was also conducted (see Experimental Section), generating a lackluster powder which is very different from the dried **Co-sheet** with film texture and metallic luster as displayed in Figure 2b–c. It suggests a 2D structure of the nanosheet, with respect to the one-phase as-made powder showing a bulk-like texture instead. Both the scanning electron microscopy (SEM) and powder X-ray diffraction (PXRD) data provided evidence of that (*vide infra*). **Co-sheet** cannot be dissolved in either organic solvent or aqueous solution, in agreement with the 2D polymeric structure as proposed in Figure 1. Besides, it is stable both in air and in solution (see Figure S2). The thermostability of **Co-sheet** was studied by thermogravimetric analysis (TGA) (Figure S2). Only 15% weight was lost when the temperature was increased to 500 °C.

The excellent thermostability of **Co-sheet** should originate from the robustness of the coordination bond between tpy and Co^{2+}.

Apart from the good stability, another advantage of **Co-sheet** is the ease of preparation and deposition process. The as-prepared large-sized nanosheet could be directly and completely transferred onto various substrates or collected with a tweezer from the interface, which could get rid of the risk of redissolution (Figure 2d and Movie in the SI). The collected **Co-sheet** could be re-suspended in the solvent again. Compared with the soluble 1D polymers and molecular materials, which usually need spin coating[42–44] or chemical bonding[45,46] in post-processing, this simple preparation and post-treatment could lower the production cost which hold a great promise for the nanosheet in different areas of applications.

2.2. Characterization of Co-sheet

The optical microscopy (OM) image (**Figure 3**a) shows the monolithic transparent yellow **Co-sheet** on a quartz substrate with a large domain (more than 1 cm in one side). The wrinkles and folded regions within the nanosheet, caused by the transfer process onto the substrate, are further emphasized in the dark field image (Figure S4), indicating the sheet-like structure of **Co-sheet**.[41,47,48] The field-emission scanning electron microscopy (FE-SEM) images (Figure 3b and Figure S5) further reveal the film-like morphology of the nanosheet as proposed in Figure 1. The twisting and folding of the nanosheet edge, which is considered as a sign of sheet material, was observed by transmission electron microscopy (TEM) (Figure 3c). **Co-sheet** also displays a uniform texture and a step terrace on the edge (Figure S6). The stair-stepping morphology reveals the layer-by-layer stacking and thus further ensures the layered structure and the bottom-up growth. The atomic force microscopy (AFM) image of **Co-sheet** shows that the selected region features a smooth and flat surface (Figure 3d). The three-dimensional (3D) AFM image further shows that **Co-sheet** is evenly spread out on the

Si substrate (Figure S7). The cross-sectional analysis result reveals the thickness of **Co-sheet** to be around 160 nm. Compared with **Co-sheet**, the one-phase made powder, which is composed of multiple, closely packed, micrometre-sized flakes, co-existing with barely dispersible bulk particles, shows a bulk-type morphology (Figure S8). Therefore, the interface-assisted synthesis not only limits the dimensions in the stacking direction, but also suppresses the growth of the bulk particles.

The sheet morphology of **Co-sheet** was verified by diverse microscopic techniques while the chemical compositions and coordination bonds were investigated by Energy Dispersive X-ray Spectrometer (EDX), X-ray Photoelectron Spectroscopy (XPS) and Fourier Transform Infra-red Spectroscopy (FT-IR). The SEM-assisted EDX in the mapping mode was used to detect the elemental composition and distribution of **Co-sheet**. The EDX-mapping images (Figure 3e) reveal the constitutive elements C, N, Co and Cl, as well as the compositional homogeneity of **Co-sheet** as desired. The obtained ratio of N: Co: Cl (6: 1.03: 1.89) is similar to the ideal stoichiometric value (6: 1: 2). XPS was conducted to characterize the nanosheet too. To make a reference, a small model molecule $[Co(tpy)_2](BF_4)_2 \cdot H_2O$ (hereinafter called **R**) was synthesized. By comparing the full spectra of the ligand **Tetra-tpy**, **Co-sheet** and the referential complex **R** (Figure S9), it could be concluded that the elements Co and Cl were incorporated into the nanosheet through complexation. Excluding the Si and O atoms respectively from the substrate and atmosphere, the revealed constitutive elements of **Co-sheet** are in good agreement with the EDX result. The narrow scan XP spectra focusing on the N 1s, Co 2p and Cl 2p core levels are displayed in **Figure 4**. The peak shift of N 1s between **Tetra-tpy** (398.57 eV) and **Co-sheet** (399.84 eV) manifests that the tpy functional groups of **Tetra-tpy** were coordinated with Co(II) ions to form **Co-sheet** and the absence of shoulder peaks for N 1s reflects the completion of complexation, considering the limit of detection for XPS (around 0.1–1 atom %). Besides, the binding energies of both N 1s and Co 2p core level of **Co-sheet** were correspondingly very similar to that of **R** (N 1s peak at 399.69 eV),

providing further evidence of the formation of the tpy-Co(II) complex motif within **Co-sheet**. The Cl 2p peak of **Co-sheet** located at 197.70 eV confirms the presence of the counterion Cl^- and the peak of **R** at 193.39 eV should be attributed to the B 1s core level. Element abundance of **Co-sheet** was analyzed by using **R** and $CoCl_2$ as standard molecules, acquiring the ratio of N: Co: Cl (6: 1.18: 1.84) which also conforms to the ideal value (6: 1: 2). In contrast, the aforementioned one-phase as-synthesized powdery product yielded the ratio of 6: 0.54: 1.02 for N: Co: Cl. The result reveals the existence of the uncoordinated tpy moieties within the one-phase made bulk powder, which presumably leads to structural defects or fragmentation of the bulk powder material, thereby underscoring the superiority of the interface-assisted method. FT-IR was also carried out to confirm the formation of the coordination bond. From the FT-IR spectra (Figure S10), the C=C stretching peak of **Tetra-tpy** was observed at 1583 cm^{-1} and shifted up to 1608 cm^{-1} after complexation with Co^{2+} to generate **Co-sheet**. This is a typical phenomenon for terpyridine when it is coordinated with the metal ion. The complexation could also be verified by the fact that the C=C stretching peak of **R** at 1600 cm^{-1} is similar to that of **Co-sheet**. PXRD patterns for both **Co-sheet** and the one-phase as-synthesized powder were obtained as shown in Figure S11. Only two broad peaks were observed in the PXRD profile of **Co-sheet** at 10.98° and 22.76°, corresponding to the interlayer distances of 8.05 and 3.90 nm, respectively. None of the additional Bragg diffraction peaks of the one-phase as-made powdery counterpart were detected, reflecting that **Co-sheet** exhibits a strong preferential orientation. Such observations further imply the 2D structure of **Co-sheet**.[49,50] The Brunauer-Emmett-Teller (BET) tests were conducted for both **Co-sheet** and the one-phase as-synthesized powder to investigate their adsorption-desorption behavior (Figure S12). Both of them show type IV isotherms. The specific surface area of **Co-sheet** was calculated to be 9.94 $m^2 g^{-1}$, which is over 3 times higher than that of the one-phase made bulk counterpart (2.87 $m^2 g^{-1}$). Besides, the bulk-type powder shows a broader Barrett–

Joyner–Halenda (BJH) pore-size distribution, which may be related to the existence of the defects caused by the incomplete complexation of Co upon N (retrospect to the XPS analysis).

Both the lateral and vertical scales of the bottom-up **Co-sheet** are controllable. It is easy to tailor the lateral size of **Co-sheet** by simply controlling the diameter of the reaction container and thus to obtain a large-sized nanosheet (see Figure S13). To control the vertical size, the relationships between the thickness of **Co-sheet** and the reaction time, the effects of the concentrations of the ligand **Tetra-tpy** and Co(II) ion solutions were investigated, respectively (Figure S14). Then, a thinner **Co-sheet** (approximately 20 nm) was achieved by shortening the reaction time as well as lowering both of the solution concentrations of Co^{2+} ion and the ligand. (Figure S15).

2.3. Electrochemical performance of Co-sheet

Recently, Feng and co-workers reported a 2D organic polymer, which served as an excellent cathode material for lithium ion battery.[29] Their ingeniously designed polymers have symmetrical shape-persistent planar aromatic structures with redox-active sites, which is similar to **Co-Sheet**. However, high temperature and sealed atmosphere are necessary for the preparation of the polymers. In consideration of the ease of preparation, the chemical stability and layered structure of **Co-sheet**, the nanosheet was used as the active material of a cathode after being assembled into a coin cell. The lithium foil functioned as an anode while a glass microfiber film acted as a separator and 1 M $LiPF_6$ in ethylene carbonate (EC)/dimethyl carbonate (DMC)/diethyl carbonate (DEC) (w/w/w 1:1:1) as the electrolyte. The fabricated half-cell was subjected to a series of electrochemical measurements such as the cyclic voltammetry (CV), galvanostatic charge-discharge test and Nyquist impedance test with an electrochemical station at room temperature. During the charging process, electrons were transferred from **Co-sheet** electrode to Li foil, resulting in the oxidation of Co(II) to Co(III)

accompanied by the intercalation of $PF_6^{\boxtimes}$from the electrolyte into **Co-sheet** to keep it electroneutral. In contrast, the inserted anion underwent deintercalation when electrons flow into the **Co-sheet** cathode and Co(III) was reduced to Co(II) during the discharging process. The obtained CV result is shown in Figure S16. A pair of redox peaks at around 2.1 V was observed, which should be attributed to the redox reaction between Co^{2+} and Co^{3+}. The theoretical specific capacity of the **Co-sheet** based battery device was calculated to be 34 mAh $g^{\boxtimes\boxtimes}$(Figure S17). The charge/discharge profiles (**Figure 5**a) show that **Co-sheet** electrode can deliver a capacity of approximately 40 mAh $g^{\boxtimes}$ at 0.1 C, corresponding to a capacity that is consistent with the proposed 2 e^- transformation from Co(II) to Co(III) in each repeat unit. Thus, it reveals a high utilization of the redox-active sites within the nanosheet. Noteworthily, 2D COFs are usually subjected to deeply buried active sites caused by the close layer-stacking.[51] The high utilization exhibited by **Co-sheet** may be assigned to the explosion of the active sites. Besides, the profiles show one charge/discharge plateau at around 2.1 V, which is in good accordance with the redox peak in the CV curve. Figure 5b displays the cycling performance of the **Co-sheet** electrode in which the assembled battery exhibited a capacity of 43 mAh g^{-1} initially. After scanning 100 cycles at 0.1 C, the battery can still give a capacity of 39 mAh g^{-1}, corresponding to a capacity retention of 93%. The capacity fading is likely caused by the accumulation of ions in the electrodes. In addition, the coulombic efficiency is increasing over the cycling, which may be attributed to the following factors.[52] Initially, due to the large size of the anion, the partially irreversible process occurs during the anion intercalation reaction, causing the trapping effect. Additionally, the unstable solid electrolyte interphase (SEI) film is formed at the electrode, resulting in the irreversible capacity. Thus, the **Co-sheet** cathode shows a relatively low coulombic efficiency. With the SEI layer more and more stable along with cycling, the irreversible capacity is diminished and therefore the coulombic efficiency is increased. The impedance of **Co-sheet** after 1st cycle is

94 ohm while after 100 cycles, it is around 100 ohm (Figure 5c). This indicates a very little increase of the internal resistance, which means a good electrochemical stability of the **Co-sheet** electrode. The rate performance is shown in Figure 5d. When the current density is increased from 0.1 C to 1 C, the charging capacity decreases slowly from 47 mAh g^{-1} to 41 mAh g^{-1} and recovers to 46.8 mAh g^{-1} with the charge/discharge rate returning to 0.1 C, indicating a good rate capability of the **Co-sheet** electrode. Such a rate capability implies the enhanced intercalation kinetics of anion into the cathode, which may be mainly attributed to the 2D structure of this kind of nanosheets, since the 2D layered structure, relative to the bulky 3D structure, could better accommodate the mechanical stress during the intercalation/deintercalation processes of anion, and reduce the activation energy barriers of the anion intercalation/deintercalation reaction.[53] To make a contrast, the electrochemical performance of the one-phase as-synthesized powder based cathode was also studied. The results are displayed in Figure S18 and a comparative table on their electrochemical performances is made (Table S1). As seen from Figure S18a, the powder-based cathode could deliver a similar redox potential at around 2.2 V vs. Li^+/Li but with a lower capacity at 0.1 C, compared with **Co-sheet**. The higher capacity of **Co-sheet** may be related to its higher specific surface area, which could generate more active sites for accommodating anions to promote the capacity of cathode. Besides, the potential hysteresis of the one-phase as-made bulk powder sample is much higher than that of **Co-sheet**, suggesting an inferior electrochemical kinetics for the powder. The capacity retention of the one-phase as-made powder sample is 86.5% after 50 cycles at 0.1 C (Figure S18b), lower than that of **Co-sheet**. Thus, **Co-sheet** exhibits a better cycling stability. The average coulombic efficiency of **Co-sheet** (92.6%) is slightly higher than that of the bulk-type powder (91.4%), indicative of the higher reversibility of the intercalation/deintercalation of anion into **Co-sheet** during the cycling. Compared with the bulk-type powder, **Co-sheet** possesses a higher specific surface area and fewer defects, which may facilitate the diffusion of anion, and thus suppress the

trapping of the inserted anion.[53] As a result, the reversibility of the anion intercalation/deintercalation process is enhanced, which boosts the cycling stability as well as the coulombic efficiency. In addition, after 50 cycles, the increase in the impedance of the one-phase as-made powdery sample is much significant than that of **Co-sheet** (Figure S18c), showing an inferior electrochemical stability of the bulk-type powdery material which may be resulted from the structural collapse and/or disintegration. For **Co-sheet**, the good electrochemical stability may be related to its structural stability, which could prevent the irreversible decomposition of the cathode, and also promote the cycling stability. The performances of several reported cathode materials for dual-ion batteries are also summarized in Table S2 for comparison. It highlights the good cycling stability of **Co-sheet**. Besides, it is noteworthy that there are rare literature reports on 2D metal complex nanosheet applied in dual-ion battery field while the reported graphite-based cathode generally shows limited capacity and the organic cathode material also suffers from the weak long-term stability. This study sheds light on the potential utility of **Co-sheet** for dual-ion battery.

3. Conclusion

Through a mild and simple interface-mediated process, a novel four-way terpyridine ligand (**Tetra-tpy**) based bottom-up nanosheet (**Co-sheet**), with elaborately introduced redox-active tpy-Co(II) motifs, was synthesized. The 2D **Co-sheet** was characterized by various microscopic methods, EDX, XPS and FTIR, revealing the proposed layered structure. Large-sized **Co-sheet** was also easily achieved. Moreover, **Co-sheet** was insoluble in both organic solvents and water, facilitating the transfer process onto substrates. A dual-ion battery device was achieved by using **Co-sheet** as the cathode material. The nanosheet can perform a high utilization of the redox-active sites and good electrochemical stability and rate capability, relative to the corresponding one-phase as-synthesized powder, which is indicative of the superiority of the metal complex nanosheet prepared by the interface-assisted approach.

Although the obtained maximum capacitance remains to be improved, the structural tunability of this kind of nanosheets may be advantageous in further enhancing the dual-ion battery performance. The study presented here enriches the family of applicable bottom-up metal complex nanosheets and provides a new strategy toward the future design and preparation of new functional 2D nanomaterials with enhanced performance.

4. Experimental Section

*Synthesis of **Co-sheet***: **Tetra-tpy** was dissolved in dichloromethane (CH_2Cl_2) to prepare the organic solution (5.0×10^{-5} mol L^{-1}) and $CoCl_2 \cdot 6H_2O$ was used as the metal source to form the metal ion aqueous solution (5.0×10^{-2} mol L^{-1}). A small piece of pretreated substrate (such as 1 cm × 1 cm silicon and quartz) was placed at the bottom of a clean and oven-dried cylindrical vial with a volume of 50 mL and a diameter of 3.2 cm. Then, a CH_2Cl_2 solution (10 mL) of **Tetra-tpy** was added into the vial (lower layer). Next, 10 mL buffer D-I water layer and 10 mL Co^{2+} aqueous layer were carefully added above the organic phase in sequence (together as the upper layer: 20 mL) to form a water-oil interface. The whole system was kept undisturbed for 5 h under ambient conditions to let the complexation proceed to form the nanosheet. Elemental analysis of **Co-sheet**: Found, N 10.66, C 68.85, H 3.94, calculated for $C_{90}H_{58}N_{12}Co_2Cl_4$ (N 10.73, C 68.98, H 3.73), the formula of the ideal repeat unit of **Co-sheet** (see Figure S17). For the preparation of the thinner **Co-sheet**, the reaction time was 0.5 h and the solution concentrations of the ligand and Co(II) ion were 2.0×10^{-5} mol L^{-1} and 2.5×10^{-2} mol L^{-1}, respectively.

Synthesis of one-phase as-synthesized powdery product: A CH_2Cl_2 solution (80 mL) of **Tetra-tpy** (6.5 mg, 4.9 μmol) was mixed with $CoCl_2 \cdot 6H_2O$ (2.5 mg, 10.5 μmol) to be strongly stirred overnight at room temperature. Then the precipitate was filtrated out and then washed with CH_2Cl_2, D.I. water and ethanol. A yellow powder was obtained after drying *in vacuo*.

*Synthesis of [Co(tpy)$_2$](BF$_4$)$_2$ •H$_2$O (**R**):* To a water solution (10 mL) of Co(BF$_4$)$_2$•6H$_2$O (62.2 mg, 168.6 μmol), 2,2′:6′,2′′-terpyridine (85.2 mg, 366 μmol) was added. After the mixture was vigorously stirred for 5 h, the precipitate was filtered out and excess aqueous ammonium tetrafluoroborate solution (1 g in 10 mL water) was poured into the filtrate. The lustrous orange solid was precipitated and filtered. Then it was washed by a small amount of water, ice-cooled methanol and oven-dried. Finally, 15 mg of the yellow solid was obtained (12.4%). Elemental analysis: found, N 11.69, C 50.54, H 3.23; calculated for $C_{30}H_{22}N_6B_2F_8Co•H_2O$, N 11.72, C 50.25, H 3.62.

Transfer of the nanosheets onto substrates and TEM grids: Small pieces could be transferred by pipetting and dropping the suspension of nanosheets onto various substrates, which were then dried in a nitrogen blow. The samples on the copper grids used for TEM were prepared in this way. Normally, the substrates were placed at the bottom of vials before the preparation. When the nanosheets were formed, both upper and bottom layers were removed by a syringe, resulting in the deposition of the nanosheets onto the substrates. Then the modified substrates were dried *in vacuo* overnight before the measurements.

Electrochemical measurements: 40 wt% **Co-sheet**, 40 wt% conductive carbon black (Ketjen Black, KB, Wuhan Battery Plant), and 20 wt% poly(tetrafluoroethylene) (60% PTFE in deionized water, Kejing, China) were mixed together to form a homogeneous slurry. Then the slurry was rolled into a composite film (80 μm thick), which was dried at 60 °C for 24 h under vacuum. A stainless-steel 2032 coin-type cell was assembled in an argon-filled glove box (Mikrouna, super H_2O and O_2 < 0.1 ppm), using the **Co-sheet** based composite material as the cathode, a glass microfibre film (Whatman, GF/A) as the separator, and Li foil as the anode. 1 M $LiPF_6$ in EC/DMC/DEC (w/w/w 1:1:1) was used as the electrolyte. The specific capacities were calculated according to the net mass of **Co-sheet** in the electrode. For the one-phase as-made powder sample, the electrode preparation procedure is similar to that of the

nanosheet. The cycling performances were tested using a charge-discharge apparatus (Land, CT2001A) at a constant current mode, with the voltage interval of 1.0–4.0 V. Cyclic voltammograms were measured on a CHI 600a electrochemical workstation (Shanghai, China) at a scan rate of 0.05 mV s^{-1} with the potential range of 1.5–4.0 V. Electrochemical impedance spectroscopy (EIS) measurements were performed for the battery after the 1st discharging using an impedance analyzer with an electrochemical interface (Autolab PGSTAT 302, Metrohem). The applied voltage during these trials was 10 mV and the frequency range was 0.1 to 10^5 Hz.

Supporting Information

Supporting Information is available from the Wiley Online Library or from the author.

Acknowledgements

W.-Y. Wong thanks the Science, Technology and Innovation Committee of Shenzhen Municipality (JCYJ20170303160036674 and JCYJ20180507183413211), the National Natural Science Foundation of China (No. 51573151), the Hong Kong Research Grants Council (PolyU 153051/17P), the Areas of Excellence Scheme of HKSAR (AoE/P-03/08), the Hong Kong Polytechnic University (1-ZE1C) and the Endowed Professorship in Energy from Ms Clarea Au (847S) for the financial support. Z. G. Meng thanks the National Natural Science Foundation of China (No. 21701112) for the financial support.

Received: ((will be filled in by the editorial staff))
Revised: ((will be filled in by the editorial staff))
Published online: ((will be filled in by the editorial staff))

References

[1] J. C. Meyer, A. K. Geim, M. I. Katsnelson, K. S. Novoselov, T. J. Booth, S. Roth, *Nature* **2007**, *446*, 60.

[2] C. Dhakal, S. Aryal, R. Sakidja, W.-Y. Ching, *J. Eur. Ceram. Soc.* **2015**, *35*, 3203.

[3] M. Naguib, V. N. Mochalin, M. W. Barsoum, Y. Gogotsi, *Adv. Mater.* **2014**, *26*, 992.

[4] H. Cheng, T. Kamegawa, K. Mori, H. Yamashita, *Angew. Chem. Int. Ed.* **2014**, *53*, 2910; *Angew. Chem.* **2014**, *126*, 2954.

[5] K. Kalantar-zadeh, J. Z. Ou, T. Daeneke, A. Mitchell, T. Sasaki, M. S. Fuhrer, *Appl. Mater. Today* **2016**, *5*, 73.

[6] R. Ma, Z. Liu, L. Li, N. Iyi, T. Sasaki, *J. Mater. Chem.* **2006**, *16*, 3809.

[7] V. Rives, M. Angeles Ulibarri, *Coord. Chem. Rev.* **1999**, *181*, 61.

[8] B. Radisavljevic, A. Radenovic, J. Brivio, V. Giacometti, A. Kis, *Nat. Nanotech.* **2011**, *6*, 147.

[9] M. Chhowalla, H. S. Shin, G. Eda, L.-J. Li, K. P. Loh, H. Zhang, *Nat. Chem.* **2013**, *5*, 263.

[10] D. Voiry, A. Mohite, M. Chhowalla, *Chem. Soc. Rev.* **2015**, *44*, 2702.

[11] G. Eda, H. Yamaguchi, D. Voiry, T. Fujita, M. Chen, M. Chhowalla, *Nano Lett.* **2011**, *11*, 5111.

[12] A. O'Neill, U. Khan, J. N. Coleman, *Chem. Mater.* **2012**, *24*, 2414.

[13] Z. Zeng, T. Sun, J. Zhu, X. Huang, Z. Yin, G. Lu, Z. Fan, Q. Yan, H. H. Hng, H. Zhang, *Angew. Chem. Int. Ed.* **2012**, *51*, 9052; *Angew. Chem.* **2012**, *124*, 9186.

[14] H. Li, J. Wu, Z. Yin, H. Zhang, *Acc. Chem. Res.* **2014**, *47*, 1067.

[15] J. Borges, J. F. Mano, *Chem. Rev.* **2014**, *114*, 8883.

[16] Y. Li, X. Wang, J. Sun, *Chem. Soc. Rev.* **2012**, *41*, 5998.

[17] Y. Xiang, S. Lu, S. P. Jiang, *Chem. Soc. Rev.* **2012**, *41*, 7291.

[18] W. Tong, X. Song, C. Gao, *Chem. Soc. Rev.* **2012**, *41*, 6103.

[19] E.-Y. Choi, C. A. Wray, C. Hu, W. Choe, *CrystEngComm* **2009**, *11*, 553.

[20] R. Makiura, S. Motoyama, Y. Umemura, H. Yamanaka, O. Sakata, H. Kitagawa, *Nat. Mater.* **2010**, *9*, 565.

[21] E. L. Spitler, B. T. Koo, J. L. Novotney, J. W. Colson, F. J. Uribe-Romo, G. D. Gutierrez, P. Clancy, W. R. Dichtel, *J. Am. Chem. Soc.* **2011**, *133*, 19416.

[22] X.-H. Liu, C.-Z. Guan, S.-Y. Ding, W. Wang, H.-J. Yan, D. Wang, L.-J. Wan, *J. Am. Chem. Soc.* **2013**, *135*, 10470.

[23] R. Sakamoto, K.-H. Wu, R. Matsuoka, H. Maeda, H. Nishihara, *Chem. Soc. Rev.* **2015**, *44*, 7698.

[24] T. Bauer, Z. Zheng, A. Renn, R. Enning, A. Stemmer, J. Sakamoto, A. D. Schlüter, *Angew. Chem. Int. Ed.* **2011**, *50*, 7879; *Angew. Chem*. **2011**, *123*, 8025.

[25] Z. Zheng, C. S. Ruiz-Vargas, T. Bauer, A. Rossi, P. Payamyar, A. Schütz, A. Stemmer, J. Sakamoto, A. D. Schlüter, *Macromol. Rapid Commun.* **2013**, *34*, 1670.

[26] Z. Zheng, L. Opilik, F. Schiffmann, W. Liu, G. Bergamini, P. Ceroni, L. T. Lee, A. Schütz, J. Sakamoto, R. Zenobi, J. Vandevondele, A. D. Schlüter, *J. Am. Chem. Soc.* **2014**, *136*, 6103.

[27] K. Takada, R. Sakamoto, S.-T. T. Yi, S. Katagiri, T. Kambe, H. Nishihara, *J. Am. Chem. Soc.* **2015**, *137*, 4681.

[28] T. Tsukamoto, K. Takada, R. Sakamoto, R. Matsuoka, R. Toyoda, H. Maeda, T. Yagi, M. Nishikawa, N. Shinjo, S. Amano, T. Iokawa, N. Ishibashi, T. Oi, K. Kanayama, R. Kinugawa, Y. Koda, T. Komura, S. Nakajima, R. Fukuyama, N. Fuse, M. Mizui, M. Miyasaki, Y. Yamashita, K. Yamada, W. Zhang, R. Han, W. Liu, T. Tsubomura, H. Nishihara, *J. Am. Chem. Soc.* **2017**, *139*, 5359.

[29] S. Xu, G. Wang, B. P. Biswal, M. Addicoat, S. Paasch, W. Sheng, X. Zhuang, E. Brunner, T. Heine, R. Berger, X. Feng, *Angew. Chem. Int. Ed.* **2019**, *58*, 849; *Angew. Chem.* **2019**, *131*,859.

[30] M. Wang, Y. Tang, *Adv. Energy Mater*. **2018**, *8*, 1703320.

[31] J. Syzdek, M. Marcinek, R. Kostecki, *J. Power Sources* **2014**, *245*, 739.

[32] J. M. Tarascon, M. Armand, *Nature* **2001**, *414*, 359.

[33] M. Armand, J. M. Tarascon, *Nature* **2008**, *451*, 652.

[34] Z. Song, H. Zhou, *Energy Environ. Sci*. **2013**, *6*, 2280.

[35] M. E. Speer, M. Kolek, J. J. Jassoy, J. Heine, M. Winter, P. M. Bieker, B. Esser, *Chem. Commun*. **2015**, *51*, 15261.

[36] M. L. Aubrey, J. R. Long, *J. Am. Chem. Soc*. **2015**, *137*, 13594.

[37] P. Novak, K. Muller, K. S. V. Santhanam, O. Haas, *Chem. Rev*. **1997**, *97*, 207.

[38] J. Shin, M. Kim, J. Cirera, S. Chen, G. J. Halder, T. A. Yersak, F. Paesani, S. M. Cohen, Y.S. Meng, *J. Mater. Chem. A* **2015**, *3*, 4738.

[39] Z. Y. Zhang, H. Yoshikawa, K. Awaga, *J. Am. Chem. Soc*. **2014**, *136*, 16112.

[40] H. Chen, F. Guo, Y. Liu, T. Huang, B. Zheng, N. Ananth, Z. Xu, W. Gao, C. Gao, *Adv. Mater*. **2017**, *29*, 1605958.

[41] R. Sakamoto, K. Hoshiko, Q. Liu, T. Yagi, T. Nagayama, S. Kusaka, M. Tsuchiya, Y. Kitagawa, W.-Y. Wong, H. Nishihara, *Nat. Commun.* **2015**, *6*, 6713.

[42] C.-H. Chiang, M. K. Nazeeruddin, M. Grätzel, C.-G. Wu, *Energy Environ. Sci.* **2017**, *10*, 808.

[43] B. K. Singh, S. Tripathi, *J. Nanosci. Nanotechnol.* **2018**, *18*, 4160.

[44] S. Kamimura, Y. Kubo, T. Tsubota, T. Ohno, *Appl. Catal. B Environ.* **2018**, *225*, 445.

[45] H. S. S. Ramakrishna Matte, A. Gomathi, A. K. Manna, D. J. Late, R. Datta, S. K. Pati, C. N. R. Rao, *Angew. Chem. Int. Ed.* **2010**, *49*, 4059; *Angew. Chem.* **2010**, *122*, 4153.

[46] J. Yao, Z. Zheng, G. Yang, *Adv. Funct. Mater.* **2017**, *27*, 1701823.

[47] R. Sakamoto, T. Yagi, K. Hoshiko, S. Kusaka, R. Matsuoka, H. Maeda, Z. Liu, Q. Liu, W.-Y. Wong, H. Nishihara, *Angew. Chem. Int. Ed.* **2017**, *56*, 3526; *Angew. Chem.* **2017**, *129*, 3580.

[48] W. Eck, A. Küller, M. Grunze, B. Völkel, A. Gölzhäuser, *Adv. Mater.* **2005**, *17*, 2583.

[49] I. K. Moon, J. Lee, R. S. Ruoff, H. Lee, *Nat. Commun*. **2010**, *1*, 73.

[50] T. Rodenas, I. Luz, G. Prieto, B. Seoane, H. Miro, A. Corma, F. Kapteijn, F. X. Llabrés i Xamena, J. Gascon, *Nat. Mater*. **2015**, *14*, 48.

[51] F. Xu, S. Jin, H. Zhong, D. Wu, X. Yang, X. Chen, H. Wei, R. Fu, D. Jiang, *Sci. Rep.* **2015**, *5*, 8225.

[52] X. Zhou, Q. Liu, C. Jiang, B. Ji, X. Ji, Y. Tang, H. Cheng, *Angew. Chem. Int. Ed*. **2019**, doi:10.1002/anie.201814294; *Angew. Chem*. **2019**, doi:10.1002/ange.201814294.

[53] L. Zhang, L. Chen, H. Luo, X. Zhou, Z. Liu, *Adv. Energy Mater*. **2017**, *7*, 1700034.

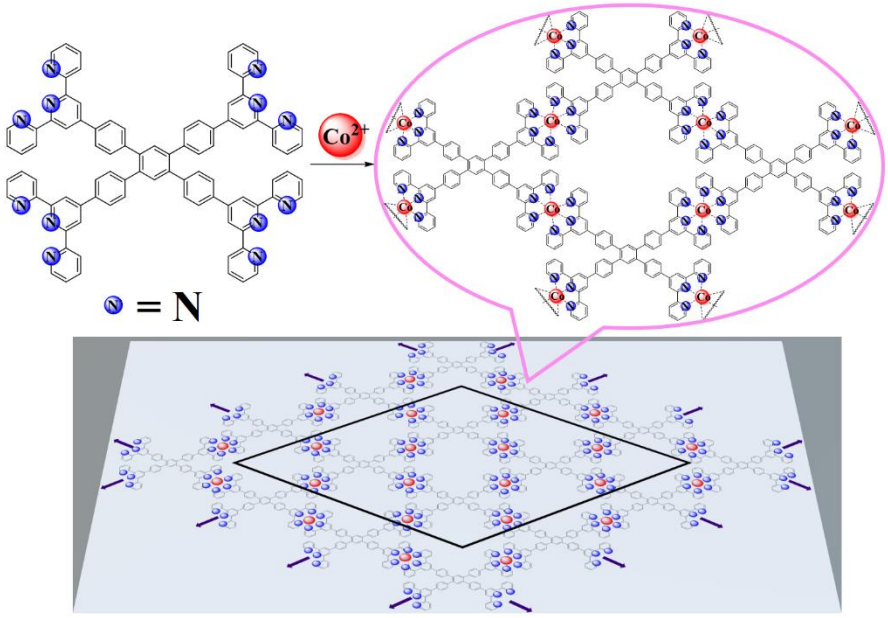

Figure 1. Chemical structure of the brand-new ligand **Tetra-tpy** and the corresponding bottom-up **Co-sheet**. The counter anions were omitted for clarity.

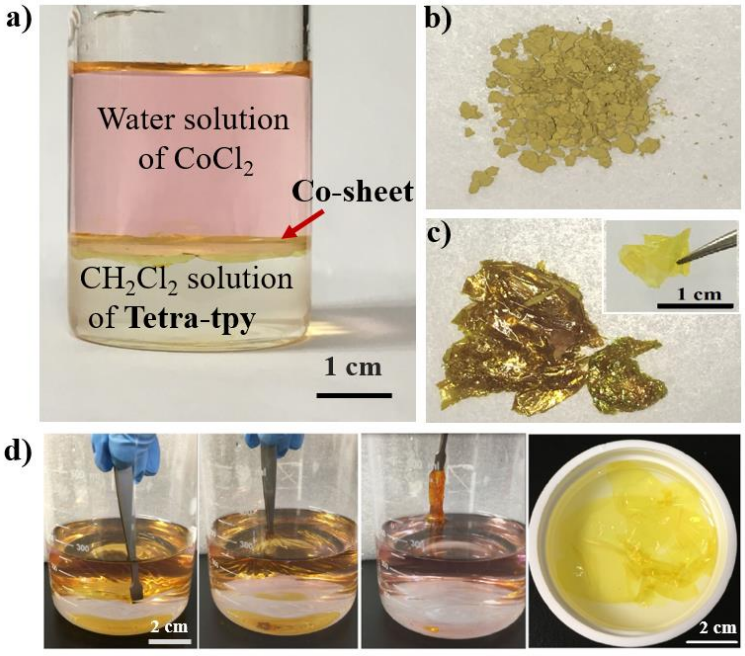

Figure 2. Preparation and collection of **Co-sheet**. a) The photograph of the nanosheet formed by the liquid-liquid interface-assisted method. b) The photograph of the solid powder synthesized through the one-phase reaction. c) The photograph of the dried **Co-sheet**. The inset is a small piece of free-standing **Co-sheet**. d) The collection of the nanosheet.

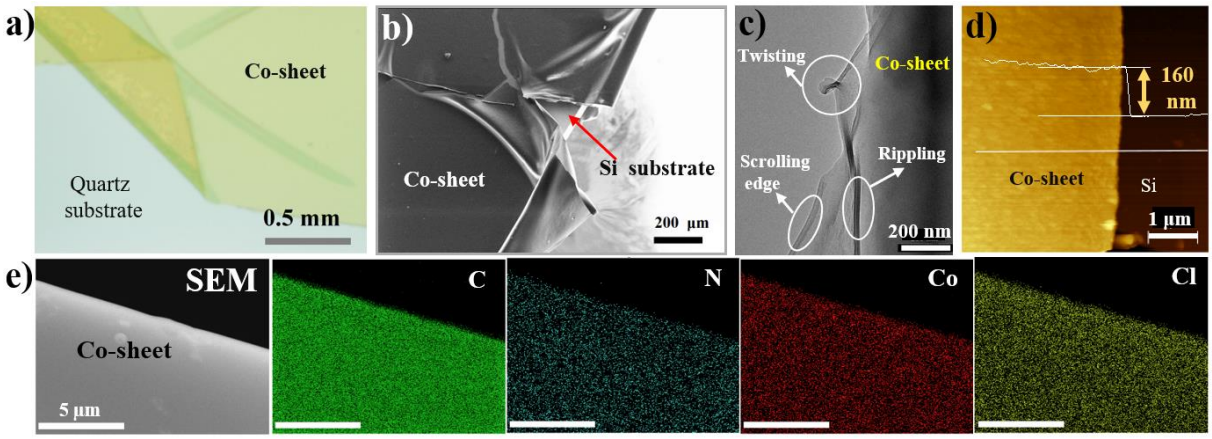

Figure 3. Characterization of **Co-sheet**. a) The OM image of the nanosheet deposited on a quartz substrate. b) The SEM image of the nanosheet deposited on the edge of the Si substrate. c) The TEM image of the nanosheet deposited on a copper grid. d) The AFM height image of the nanosheet on a Si substrate and the cross-sectional analysis along with the white line. e) The SEM/EDX mapping images of **Co-sheet**.

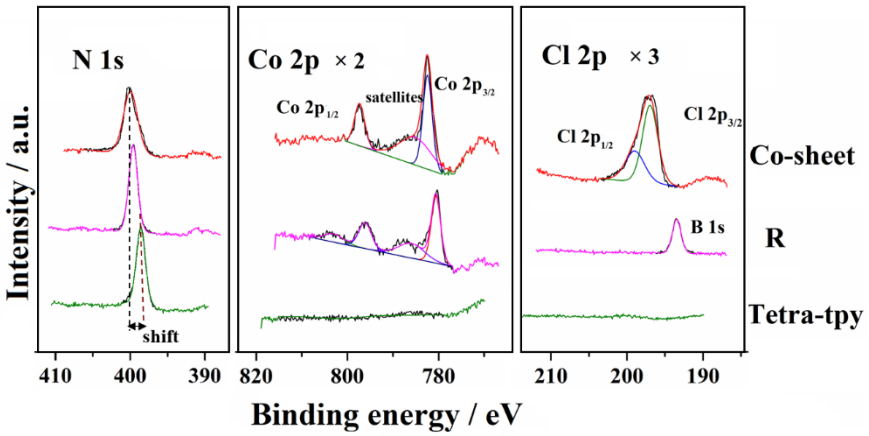

Figure 4. The narrow scan XP spectra of **Co-sheet**, referential complex **R** and **Tetra-tpy** focusing on N 1s, Co 2p, and Cl 2p core levels, respectively.

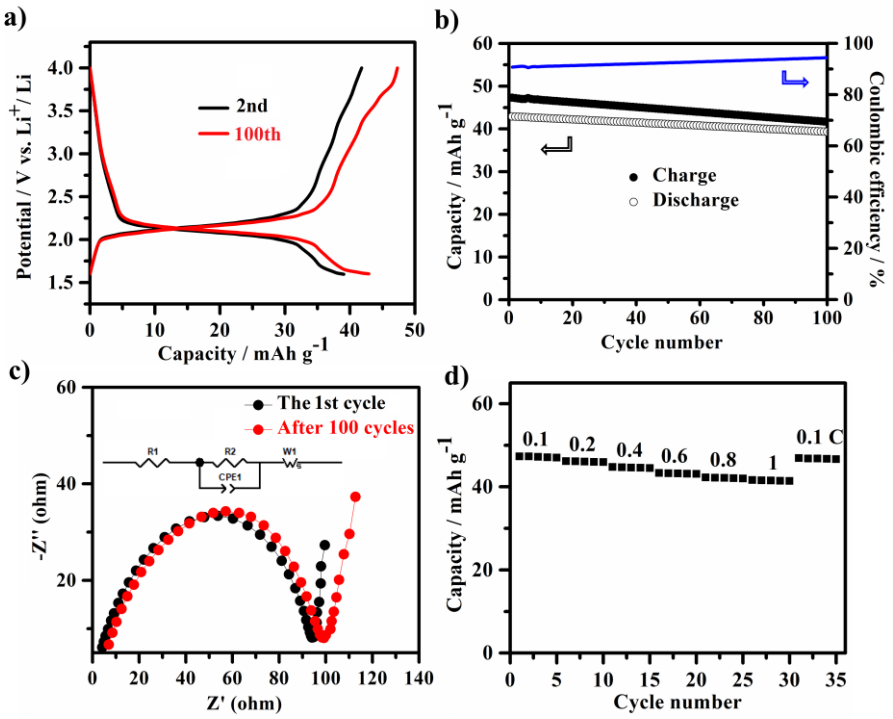

Figure 5. The electrochemical performance of the **Co-sheet** electrode. a) Charge/discharge profiles of the **Co-sheet** electrode at the 2nd and 100th cycles (0.1 C, 1 C = 34 mAh g^{-1}). b) Cycling performance of the **Co-sheet** electrode at 0.1 C. c) The AC impedance spectrum of the **Co-sheet** electrode after the 1st cycle and 100th cycles. d) Charge capacity of the **Co-sheet** electrode at different current density.

Co-sheet cathode: A novel bottom-up metal complex nanosheet, constructed by elaborately embedding the electrochemically active bis(terpyridine)-Co(II) linkages onto the skeleton, is applied as a cathode material of a dual-ion battery for the first time, presenting a high utilization of redox-active sites and good electrochemical stability and rate capability.

Keywords: metal-organic nanosheets, layered structures, cathode materials, dual-ion batteries, terpyridine

Y. R. Liu, W. W. Deng, Z. G. Meng,* W.-Y. Wong*

A Tetrakis(terpyridine) Ligand Based Cobalt(II) Complex Nanosheet as a Stable Dual-Ion Battery Cathode Material

ToC figure